Optically deep asymmetric one-dimensional plasmonic crystal slabs: Genetic algorithm approach

Masanobu Iwanaga

Department of Physics, Graduate School of Science, Tohoku University, Sendai 980-8578, Japan
Present address, Quantum Dot Research Center, National Institute for Materials Science (NIMS), 1-1 Namiki, Tsukuba 305-0044, Japan (IWANAGA.Masanobu@nims.go.jp)

Received November 19, 2008; accepted March 20, 2009;
posted March 30, 2009 (Doc. ID 104260); published April 27, 2009

Optical asymmetry with regard to transmission has been numerically explored in one-dimensional (1D) plasmonic crystal slabs (PlCSs) with the help of a genetic algorithm (GA). Optically deep asymmetric PlCSs are not obtained in one-layer systems and can be achieved in unit cell structures composed of more than two layers. The optical asymmetry is classified into two types. One is ascribed to anisotropic diffraction efficiency, and the other comes from collective oscillations of particle plasmons in each metallic nanorod and can induce nearly perfect absorption over a broad band. In both asymmetry types, the degree of freedom in depth is crucial to manipulate the linear optical responses of PlCSs. On the basis of the GA search, a simple design for optically asymmetric 1D PlCS is extracted, which provides a standard for broadband plasmonic absorbers in both photon energy and incident angles.

OCIS codes: 050.5298, 220.0220, 300.1030, 050.1950.

1. INTRODUCTION

Attempts to tailor linear optical responses in artificial structures have quite a long history, stemming from the study of diffraction gratings [1], and have been inherited by the quest for extraordinary or negative refraction in photonic crystals [2–4] and metamaterials [5,6]. In some cases, the optical designs obtained are based on the understanding of optical properties in artificial structures. For example, an efficient design for manipulating the polarization of light in subwavelength dimensions was invented [7] from physical properties such as effective refractive index [8]. In most cases, it is difficult to achieve relevant designs by handmade structural modification. Indeed, automatic searches by computational methods have often been tried and have led to optimized designs [9–15]. One flexible and robust technique is based on the genetic algorithm (GA).

The GA has already been established and has been applied to many problems in diverse fields from biology to engineering [16,17]. There have been some attempts to apply GAs to photonic structures to optimize the bandgap in 1D or 2D photonic crystals [12,13] and the effective negative index [14] and permeability [15] of metamaterials.

Optical asymmetry is hard to realize by hand. Before the details are described, some notation is prepared here. Figure 1(a) shows the optical configuration for a 1D plasmonic crystal slab (PlCS). Although a PlCS is often referred to as a metallic photonic crystal slab, the photonic eigenmodes stem from surface plasmon polaritons [18]; therefore, here the metallic periodic structure is called a PlCS. Metallic rods (gray), which are infinitely long along the y axis, are put on the substrate and are arrayed periodically along the x axis. The unit cell corresponds to the area between the vertical dashed lines. When incident light falls on the PlCS with the incident angle θ, linear optical responses T_n and R_n are induced, where T_n and R_n denote the nth transmissive and reflective diffraction efficiencies, respectively. In particular, T_0 and R_0 are ordinary transmittance and reflectance, respectively.

Diffractions T_n and R_n $(n \neq 0)$ appear and disappear, depending on the incident photon energy and angles. To explore more general situations, let us focus on transmittance T_0 and reflectance R_0; the simplified notation of T $(=T_0)$ and R $(=R_0)$ are used from now on. In the two incident configurations of Figs. 1(b) and 1(c), note that for reflection there exists the general restriction, called reciprocity, such that $R_0(\theta)=R_0(-\theta)$, which is independent of the structure in the unit cell and the incident photon energy [19]. Elementary proof of reciprocal relations was reported in [20]. The asymmetric optical response thus appears to concern transmittance in the present configuration.

Taking account of the reciprocal relation, a simple definition of the optical asymmetry parameter σ_0 is given by

$$\sigma_0 = \frac{T(\theta) - T(-\theta)}{T(\theta) + T(-\theta)}, \tag{1}$$

where θ is the incident angle and $\theta \neq 0°$. The sign of θ is defined relative to the direction of the x axis. This parameter cannot distinguish transmissive PlCS of $T(\theta)=1$ and $T(-\theta)=0.01$ from reflective PlCS of $T(\theta)=10^{-3}$ and $T(-\theta)=10^{-5}$. In both cases, Eq. (1) results in $\sigma_0=0.98$. To avoid such undesirable degeneracy, a modified asymmetric parameter σ is defined as the following:

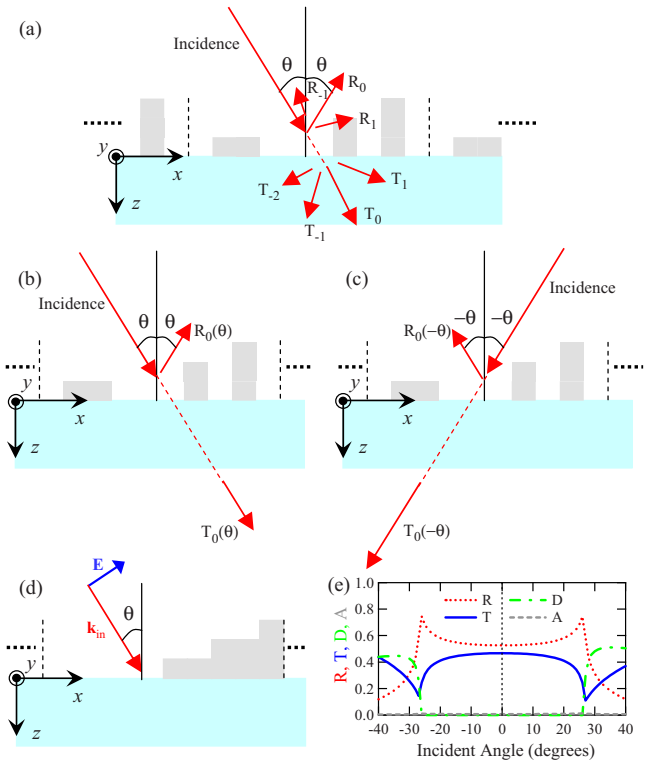

Fig. 1. (Color online) (a) Schematic drawing of the xz section of 1D PlCS and optical configuration. The unit cell of 1D PlCS is defined in the area between the vertical dashed lines. The 1D PlCS is periodic along the x axis and infinitely long along the y axis. In accordance with the coordinates, the diffraction channels T_n and R_n are labeled. (b) and (c) are reciprocal concerning reflection R_0 with each other. (d) A structurally asymmetric 1D PlCS. (e) Optical spectra of (d) at 1.3 eV, dependent on incident angles under p polarization. Reflectance (R), transmittance (T), total diffraction efficiency (D), and absorption (A) are displayed with dotted red, solid blue, dashed-dotted green, and dashed gray lines, respectively. Note that A is close to zero.

$$\sigma = |T(\theta) - T(-\theta)|[1 - R(\theta)]. \quad (2)$$

The parameter σ in Eq. (2) discriminates transmissive PlCS from reflective PlCS and gives larger value to optically asymmetric and transmissive PlCS; σ is suitable for characterizing the optical asymmetry in transmission.

As is mentioned above, the optical asymmetry is not easily obtained by thinking of structurally asymmetric 1D PlCSs. The unit cell in Fig. 1(d) is structurally asymmetric; the periodicity is 500 nm, the height of each step is 40 nm, and the metal is set to be silver. The optical constant of silver was taken from the literature [21]. The substrate is assumed to be quartz, which has permittivity of 2.13. When incident light is p polarized (i.e., the electric vector $\mathbf{E} \perp y$), the computed transmittance at 1.3 eV is almost symmetric, as is shown in Fig. 1(e) (solid blue curve), that is, $\sigma \approx 0$ at any θ of $0° < \theta \leqslant 40°$. This example evidently shows that structural asymmetry does not always come with optical asymmetry. This is one of the reasons why we execute automatic search by use of a GA: it is most likely to reach intended and realistic designs by exploring diverse unit cells. Indeed, though many efforts have been devoted to relevant designs of diffraction gratings, there has been no report on optically asymmetric PlCSs concerning transmission.

In Fig. 1(e), reflectance (dotted red curve) exhibits reciprocity. Total diffraction efficiency D, which is defined as $D = \Sigma_{n \neq 0}(T_n + R_n)$, is shown as the dashed-dotted green curve. In Fig. 1(e), only two diffraction channels, $T_{\pm 1}$, are open at $|\theta| > 26°$; hence, $D = T_1 + T_{-1}$. Absorption, which is defined as A $(=1 - T - R - D)$ (dashed gray curve), is very small and close to zero, though the filling ratio of metal in the unit cell is 33%.

The computational solver to evaluate linear optical responses is based on the Fourier modal method [22], which is improved in convergence [23] and combined with a scattering matrix algorithm [24]. In this paper the numerical fluctuation in evaluating optical responses was kept to less than 1% by use of a large number of Fourier harmonics.

In this paper, the aim is to find optically deep asymmetric 1D PlCSs by use of a GA. In particular, practical structures of PlCS are sought, avoiding the most asymmetric but impractical structures. Moreover, I extract clear physical pictures of the origin of deep optical asymmetry in 1D PlCSs. The scheme of the simple GA (SGA) is described in Section 2. The purely numerical results obtained by the SGA search are shown in Subsections 3.A–3.C. Based on the SGA results, more realistic structures that can be fabricated by contemporary nanofabrication techniques are examined in Subsection 3.D. The features of large-σ PlCSs are discussed in Section 4.

2. GENETIC ALGORITHM SEARCH

Figure 2 provides an illustration of the SGA. A chromosome here corresponds to an unit cell of a 1D PlCS on an infinitely thick quartz substrate. In Fig. 2, an unit cell is

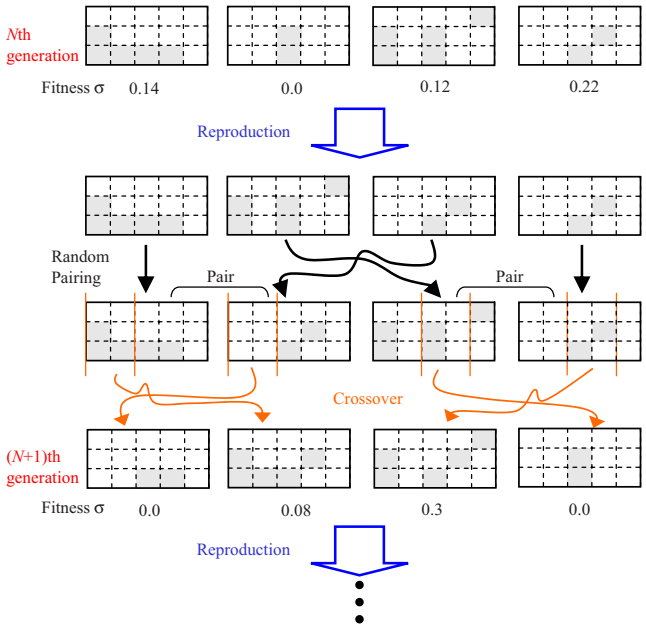

Fig. 2. (Color online) Scheme of SGA. Each unit cell (or chromosome) in the Nth generation is evaluated by fitness σ, and then a tentative set of unit cells are reproduced in proportion to their fitness. Random pairing is executed. Each pair does crossover by exchanging a part of each unit cell. The part is the area between orange vertical lines. The next $(N+1)$th generation is finally produced. Succeeding generations are produced similarly.

composed of 5×3 grid elements. Each grid element is filled with silver or air, so that a unit cell has 2^{15} possible combinations. The scheme for the SGA, comprising reproduction, pairing, crossover, and mutation, is as follows.

Let us consider the case that each generation has four populations as shown in Fig. 2. When the Nth generation is given, every unit cell is evaluated by fitness. In the present case, the fitness is the asymmetric parameter σ in Eq. (2). A 1D PlCS is constituted by the unit cell on the quartz substrate as shown in Fig. 3(a). Linear optical responses of the PlCS are computed at a given photon energy and incident angles (θ and $-\theta$), and the fitness is evaluated by use of Eq. (2).

1. *Reproduction*. A set of unit cells is reproduced in proportion to its fitness. Unit cells that have larger σ tend to be generated more often. Unit cells of $\sigma=0$ are terminated in the reproduction.
2. *Pairing*. After reproduction, random pairing of unit cells is made.
3. *Crossover*. Each pair exchanges a part (or parts) of the unit cell as shown in Fig. 2. The cutting positions (orange vertical lines) are randomly determined for each pair. The way of cutting is in accordance with the *building block hypothesis*, which assumes that a block (or blocks) of the unit cell is responsible for the larger fitness [17]. Crossover is thus executed by exchanging a block from the unit cell and produces the next $(N+1)$th generation.
4. *Mutation*. A part (or parts) of the unit cell is randomly chosen with a small probability ($\sim$0.02, for example) and reversed; silver is replaced with air and vice versa.

Mutation plays a role when a generation comes to saturation, that is, when a generation is filled with the same unit cell. Then, any crossover obviously produces the same unit cell. In the present SGA search, the simple mutation, which reverses constituents in a randomly chosen block in the unit cell, tends to destroy the building block and to result in a decrease of σ. As shown in Section 3, we can obtain large-σ unit cells before mutation plays a role.

Figure 3 shows a typical result of the SGA search. Each grid element has the dimension of 50 nm$\times$40 nm along the x and z axes, respectively. The incident photon energy was 1.65 eV. Incident angles were 30° and −30°. A SGA search was executed for 12 generations and 600 populations in each generation. Since here I intend to execute automatic search, the initial set of unit cells was chosen randomly. The average of fitness σ in each generation is shown with red open circles in Fig. 3(b). The average

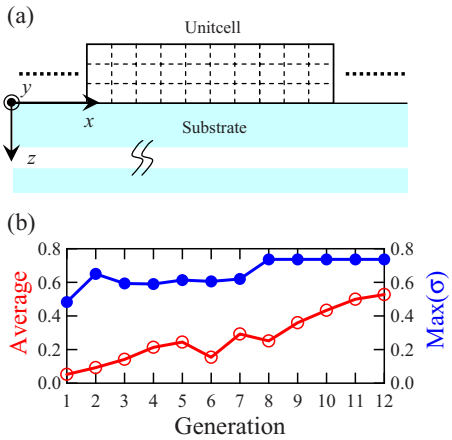

Fig. 3. (Color online) Configuration of unit cell and a typical result of SGA search. (a) Actual configuration in the SGA search. The unit cell is located on an infinitely thick substrate and periodically arrayed along the x axis. The unit cell is infinitely long along the y axis. (b) Average (red open circles) and the maximum (blue closed circles) of σ at each generation, which has a population of 600. The photon energy was set to be 1.65 eV, and incident angles were ±30°.

gradually increases in proportion to the generation and has a ten times larger value at the twelfth generation in comparison with the first generation. SGA thus works successfully to produce good unit cells. The maximum in each generation is plotted for the right axis with blue closed circles. The largest σ is obtained at the eighth generation and is reproduced later. Note that the unit cell of largest σ is realized through the SGA search. These results indicate that the SGA efficiently finds good unit cells for the present goal.

3. NUMERICAL RESULTS

A sequence of systematic trials to seek optically asymmetric 1D PlCSs is described in Subsections 3.A–3.C. The periodicity is set to be 500 nm, and the size of the grid element in the unit cell is defined as 50 nm$\times$50 nm. The unit cell is therefore divided into ten sections along the x axis. PlCSs of m layers have $10\times m$ grids in the unit cell. The results for one, two, and three layers are described in Subsections 3.A–3.C, respectively. The photon energy is fixed at 2.0 eV (619.8 nm in wavelength) and the incident angles are taken at ±40°. Under this condition, the diffraction channels of $T_{\pm 1}$ and $R_{\pm 1}$ are open. Incident light is p polarized.

In Subsection 3.D, a simple PlCS of deep optical asymmetry is designed based on the results of the SGA search. The underlying physics of the deep optical asymmetry is studied.

A. Unit Cell of One Layer

The division along the z axis is one. The total grid elements in the unit cell are 10; possible combinations in the unit cell are 2^{10} (=1024). With such a small number of combinations every case could be explored. However, the SGA search was executed with the conditions that the generations are 5 and the populations are 1200; the large population is intended to execute the search for every case. As a result, the maximum was found to be very small and was less than 0.01. Single-layer 1D PlCSs are thus far from optical asymmetry.

B. Unit Cell of Two Layers

In this case, the grid elements in the unit cell are 10×2, and the total possible combinations are 2^{20} ($\approx 10^6$). It is not practical to evaluate every combination. An SGA search was performed with the condition that the total generations are 12 and populations at each generation are 600.

Figure 4 displays typical results of SGA searches, which were repeated by changing the initial set of unit cells. Figure 4(a) is the unit cell of an asymmetric PlCS of $\sigma=0.19$. The optical spectra at 2.0 eV is shown in Fig. 4(b). Transmittance (solid blue) exhibits the asymmetry connected to the asymmetry of diffraction efficiency (dashed-dotted green) and absorption (gray dashed). Optically asymmetric 1D PlCS are thus realized in most cases.

Figure 4(c) presents a PlCS of large $\sigma=0.56$. Asymmetry in transmittance is clearly seen; the transmittance at −40° is 0.81, and that at 40° is 0.20. From Fig. 4(d), the asymmetry is attributable mainly to the asymmetric absorption.

We note that the optical asymmetry in Fig. 4(c) is associated with large absorption. The filling ratio of metal in the unit cell is 30% in Fig. 4(c) and less than that in the unit cell in Fig. 4(a). Nevertheless, absorption is significantly large at $\theta\geqslant 40°$ in Fig. 4(c). This result indicates that light absorption can be controlled by the unit cell structures. Also, in comparison with the one-layer results in Sec. 3.A, it is obvious that the PlCSs of two layers can have high optical asymmetry.

C. Unit Cell of Three Layers

The unit cell of three layers has 10×3 grids and can represent 2^{30} ($\approx 10^9$) combinations. It is actually impossible to evaluate the fitness in every case. An SGA search was done with the condition that total generations are 12 and the population in each generation is 600.

Figure 5 shows PlCSs of large fitness and the corresponding optical spectra. Figure 5(a) presents a PlCS of $\sigma=0.68$; the metallic part is simply connected. The optical spectra are shown in Fig. 5(b); the notation is the same as in Fig. 1(e). Reflectance (dotted red) and absorption (dashed gray) are quite suppressed. Transmittance (solid blue) and total diffraction efficiency (dashed-dotted green) are nearly symmetric for incident angles of $\theta>20°$. This is a typical representation of optical asymmetry, that is, the trade-off type of transmission and diffraction.

Figure 5(c) is a PlCS of $\sigma=0.76$, which is very large fitness. The unit cell is quite complicated and consists of four separated metallic parts. Transmittance is deeply

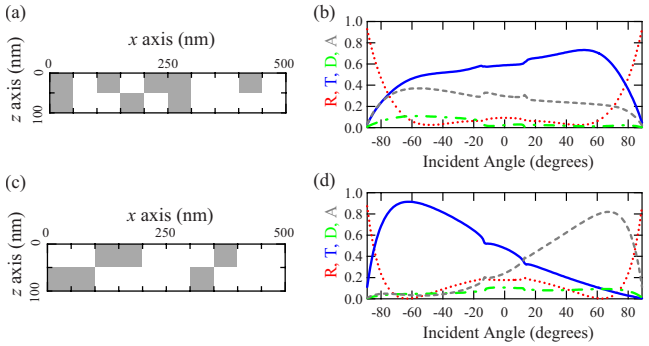

Fig. 4. (Color online) (a) An optically asymmetric two-layer 1D PlCS of $\sigma=0.19$ and (b) the optical spectra at 2.0 eV, in which the notation is similar to Fig. 1(e). (c) Highly asymmetric two-layer unit cell of $\sigma=0.56$, searched by SGA and (d) the optical spectra at 2.0 eV.

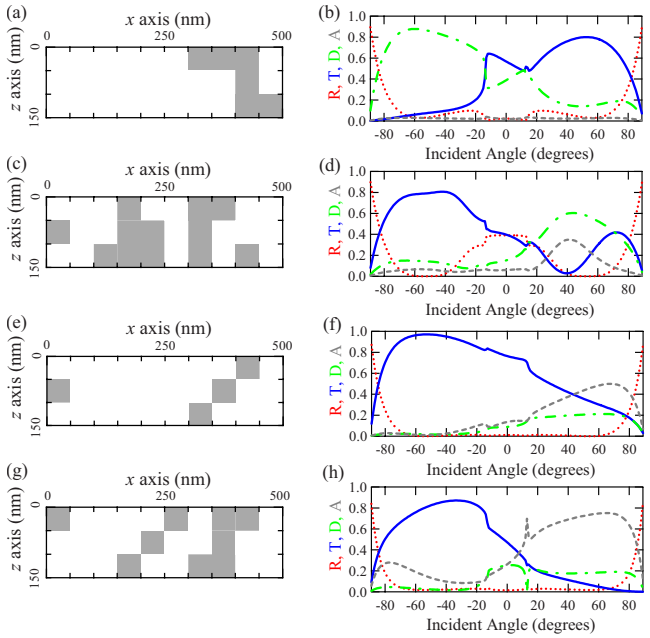

Fig. 5. (Color online) Optically highly asymmetric three-layer 1D PlCSs found by SGA, and the linear optical spectra: (a) unit cell of $\sigma=0.68$, (b) optical spectra of (a) at 2.0 eV, dependent on incident angles. The notation of optical spectra is similar to Fig. 1(e). Similarly, (c) unit cell of $\sigma=0.76$, and (d) the optical spectra of (c). (e) unit cell of $\sigma=0.53$, and (f) the optical spectra of (e). (g) unit cell of $\sigma=0.74$, and (h) the optical spectra of (g).

asymmetric; $T=0.81$ at $-40°$ and $T=0.01$ at $40°$. Optical spectra in Fig. 5(d) shows that this unit cell is optimized to realize $T\approx 0$ at $40°$. The nearly zero transmittance is associated with the enhancement of diffraction and absorption. In addition, note that reflectance is well suppressed from $40°$ to $60°$.

Figure 5(e) is a PlCS of $\sigma=0.53$. The unit cell is not well optimized but exhibits a remarkable feature: transmittance at $-40°$ is almost 100% and is significantly reduced at $40°$, as shown in Fig. 5(f). Besides, reflectance is well suppressed in a wide range of incident angles. Qualitatively, when the incident wave vector is parallel to the steplike array of metallic rods ($\theta\sim -45°$), efficient transmittance is realized. On the other hand, when the incident wave vector is perpendicular to the steplike array ($\theta\sim 45°$), absorption increases with reducing transmittance. Large fitness is thus obtained through the trade-off of transmission and absorption. This is another type of PlCS for realizing deep optical asymmetry, different from the type in Fig. 5(a). As for the filling ratio of metal and the absorption, the unit cell of Figs. 5(a) contrasts with that of Fig. 5(e); the filling ratio is larger in the former, but light absorption is clearly large in the latter. This result strongly suggests that the structure in the unit cell is crucial for inducing large light absorption, and the ratio of metal is inessential.

Figure 5(g) displays a PlCS of large $\sigma=0.74$, which can be regarded as a better unit cell than that in Fig. 5(e). The contrast of T at $40°$ and $-40°$ is quite high. Absorption is also modified and reaches about 70% at $40°$. Figures 5(e) and 5(f) imply that the steplike structure is the building block to realize the optical asymmetry connected with large absorption.

From a purely numerical viewpoint, it would attract interest to explore the unit cells of ultimate large fitness $\sigma=1$. To execute a further search, it is probably necessary to divide the present grid elements into finer subgrid elements, as was done in [12]. Such a method of optimization is not based on GA and is the usual way of finding the maximum. However, here I concentrate on designing simple and practical unit cells by exploiting the building block found in the SGA search, and I examine the PlCS of a four-layer unit cell in the next subsection.

D. Unit Cell of Four Layers

In Subsections 3.A–3.C, the results of SGA search have been described. The search is purely numerical and is not always intended to obtain practically feasible structures. In this subsection, we study optically deep asymmetric 1D PlCS of a four-layer unit cell that are simultaneously practical.

Figure 6(a) shows the unit cell designed by hand, based on the result by SGA search. The grid size is 50 nm $\times$50 nm, and the area between vertical dashed lines consists of 10×4 grid elements. To ensure the feasibility of nanofabrication, all the metallic rods are supported by substrate and form simple unit cells. Indeed, 50 nm lines can be fabricated by contemporary nanofabrication techniques, and the depth control is also within reach. Double steplike structures in the area between the vertical dashed lines have two meanings: (i) the increase in absorption and (ii) the termination of diffraction at 2.0 eV by shorting the periodicity. Nearly perfect absorption is observed at $-30°$ in Fig. 6(b). Transmittance exhibits strong contrast at $40°$ and $-40°$. The fitness σ is 0.48 and remains a quite large value.

The origin of the nearly perfect absorption in Fig. 6(b) is examined from the electromagnetic distributions in Figs. 6(c) and 6(d). Under p polarization, the magnetic component H_y is parallel to the metallic rods. As shown in

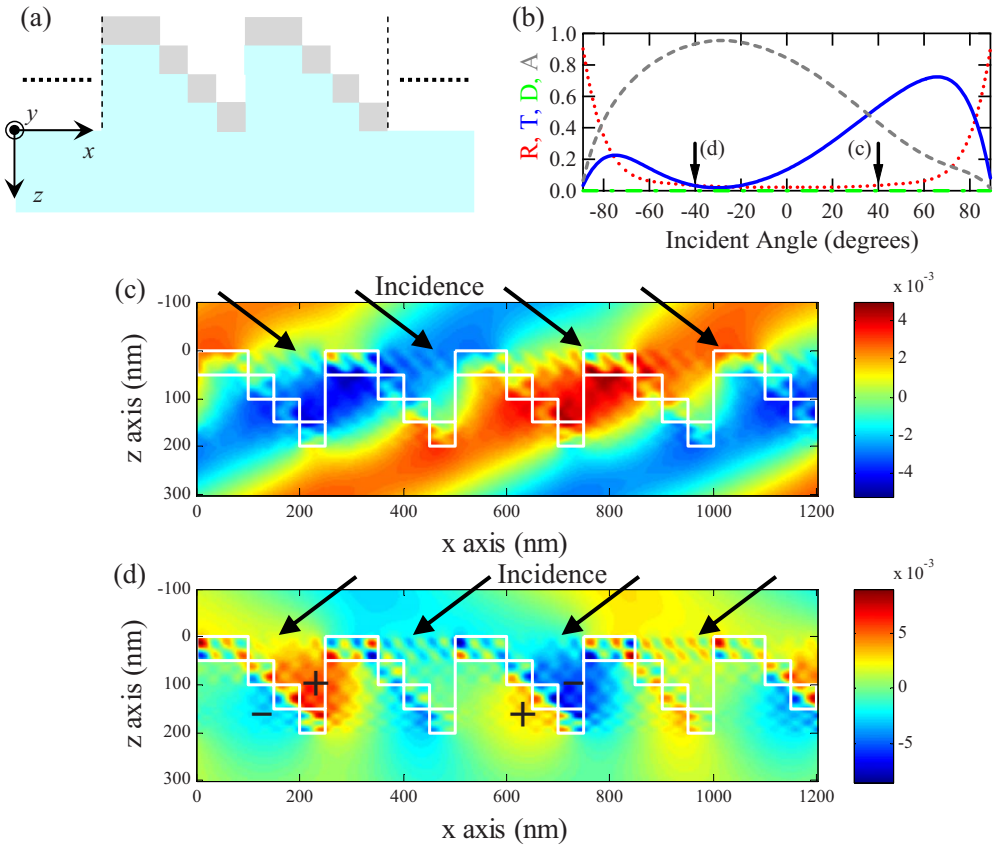

Fig. 6. (Color online) Optically highly asymmetric four-layer 1D PlCS, which is designed by hand on the basis of the results of SGA search. (a) Unit structures. (b) Optical spectra at 2.0 eV; the notation is similar to Fig. 1(e). (c) and (d) Snapshots of H_y distributions at 40° and −40°, respectively. The scale is determined by the definition such that the magnitude of incident electric field $|\mathbf{E}_{in}|$ is equal to unity. Arrows indicate the direction of incident wave vectors.

Fig. 6(c), although the H_y distribution is modulated in the 1D PlCS at the incident angle of 40°, incident light travels through the PlCS. On the other hand, the H_y distribution is very different at −40° as shown in Fig. 6(d). Plasmonic oscillations, which are usually called particle plasmons, are seen in each metallic rod (the rectangular areas inside the white lines); the properties of particle plasmons in metallic nanorods were studied in [25]. The large-area uncommon oscillations, which has the directions designated by the signs ± in Fig. 6(d), spread outside each metallic rod and are induced by collective oscillations of the particle plasmons that resides inside metallic nanorods. We call the new collective modes *large plasmons*. The large plasmons induce the large light absorption.

We again refer to the fact that the one-layer unit cell does not show large absorption, as noted in Subsection 3.A; this fact is consistent with the absence of the large plasmons in the one-layer PlCSs. The large plasmons cannot be induced by a single nanorod. The minimum requirement to induce the large plasmons is two-layer unit cell. Indeed, Figs. 4(c) and 4(d) show quite large absorption, which is the signature of large plasmons. Such a collective mode of particle plasmons has not been reported to our best knowledge.

Figure 7(a) shows an unit cell similar to Fig. 6(a) but the metallic parts are firmly connected. The size of grid elements is 25 nm × 25 nm, and the area between vertical dashed lines has 20 × 8 grids. The unit cell of the 1D PlCS is obviously asymmetric in structure, and nevertheless the PlCS is almost symmetric optically as shown in Fig. 7(b). Transmittance (solid blue) shows a high value of about 0.8 at 40° and −40°, and absorption (dashed gray) is suppressed down to 0.1. Figure 7 is a simple but clear example that shows that the large plasmons are very sensitive to the structure in the unit cell.

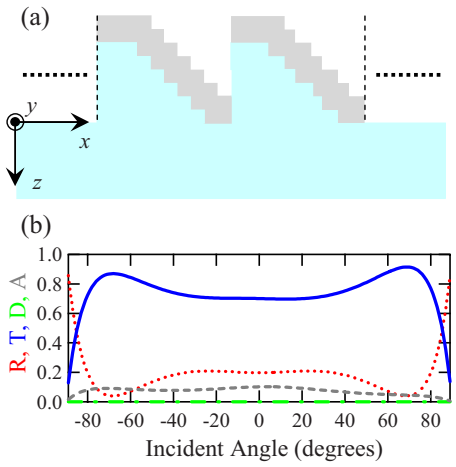

Fig. 7. (Color online) (a) Structurally asymmetric 1D PlCS designed to compare with Fig. 6(a). (b) Optical spectra at 2.0 eV; the notation is similar to Fig. 1(e).

4. DISCUSSION

In this section I discuss the features of the PlCS in Fig. 6 in comparison with the other light absorbers.

Total absorption by diffraction gratings is a rather well-known phenomenon [26]. However, the total absorption has a very narrow linewidth; the width of $A>0.9$ is less than 0.5° in incident angle. In contrast, absorption of over 90% takes place at the broad angles from −45° to −5° in Fig. 6(b).

Furthermore, the nearly perfect absorption by the PlCS in Fig. 6(a) has quite a wide range in energy; the absorption of $A>0.9$ holds at 1.5–2.2 eV under the incident angle of −40°. The range is more than ten times wider than the energy range of $A>0.9$ in mesoporous gold, which exhibits omnidirectional perfect absorption [27]. As a light absorber, the 1D PlCS in Fig. 6(a) thus has the advantage in the broadband features of both energy and incident angles.

The efficient absorption energy band of the PlCS in Fig. 6(a) does not show any prominent peak, that is, any discrete energy level that is the signature of bonded states of particle plasmons in metallic nanorods [28]. Instead, it is suggested that the large plasmons form a new continuum that is subradiant.

The PlCS in Fig. 6(a) has anisotropic subradiant plasmonic mode, that is, large plasmons, whereas the PlCS in Fig. 7(a) shows efficient radiation at all the incident angles. From the comparison of the two PlCSs, it is evident that the radiation from PlCSs to the outer far field can be controlled just by modifying the unit cell structures by a small amount. The PlCSs in Figs. 5(a) and 7(a) are highly radiant and imply the general tendency that the PlCSs with firmly connected metallic part(s) in the *xz* section of the unit cell are efficiently coupled with the far field. We also note that the PlCS in Fig. 1(d) is consistent with the general tendency; it is highly radiant and has little absorption, as is shown in Fig. 1(e).

Light absorption due to metallic structures can enhance photocurrent when the metallic structures are coupled with semiconductors [29]. Thus, the perfect absorber based on the present SGA search would also be useful to enhance photocurrent and photovoltage as a constituent of a relevant device together with semiconductors.

5. CONCLUSIONS

Optically deep asymmetry has been numerically explored in 1D PlCSs with SGA. Unit cell structures of large fitness are not realized in one-layer 1D PlCSs and have been found in two- or three-layer 1D PlCSs. The large fitness, that is, the deep optical asymmetry, is obtained by two ways: one is connected to anisotropic diffraction efficiency, and the other is due to anisotropic large absorption. The building block of the latter has been employed to design a simple plasmonic absorber. It has been clarified that the large light absorption originates from large plasmons, which are collective oscillations of the particle plasmons that exist in each metallic nanorod. It has also been shown that the structures constituted by metallic nanorods are essential to induce the large plasmons. The present design based on the SGA search will be a representative of broadband light absorbers of 1D PlCS.

ACKNOWLEDGMENTS

This work is partially supported by the Research Foundation for Opto-Science and Technology and by Dean's Grant for Exploratory Research (Graduate School of Science), and by Cyberscience Center, Tohoku University.

REFERENCES

1. M. Born and E. Wolf, *Principles of Optics*, 7th ed. (Cambridge U. Press, 1999), p. 446.
2. H. Kosaka, T. Kawashima, A. Tomita, M. Notomi, T. Tamamura, T. Sato, and S. Kawakami, "Superprism phenomena in photonic crystals," Phys. Rev. B **58**, R10096–R10099 (1998).
3. M. Notomi, "Theory of light propagation in strongly modulated photonic crystals: refractionlike behavior in the vicinity of the photonic band gap," Phys. Rev. B **62**, 10696–10705 (2000).
4. T. Decoopman, G. Tayeb, S. Enoch, D. Maystre, and B. Gralak, "Photonic crystal lens: from negative refraction and negative index to negative permittivity and permeability," Phys. Rev. Lett. **97**, 073905 (2006).
5. A. J. Hoffman, L. Alekseyev, S. S. Howard, K. J. Franz, D. Wasserman, V. A. Podolskiy, E. E. Narimanov, D. L. Sivco, and C. Gmachl, "Negative refraction in semiconductor metamaterials," Nature Mater. **6**, 946–950 (2007).
6. J. Valentine, S. Zhang, T. Zentgraf, E. Ulin-Avila, D. A. Genov, G. Bartal, and X. Zhang, "Three-dimensional optical metamaterial with a negative refractive index," Nature **455**, 376–380 (2008).
7. M. Iwanaga, "Ultracompact waveplates: approach from metamaterials," Appl. Phys. Lett. **92**, 153102 (2008).
8. M. Iwanaga, "Effective optical constants in stratified metal-dielectric metamaterial," Opt. Lett. **32**, 1314–1316 (2007).
9. Y. Chen, R. Yu, W. Li, O. Nohadani, S. Haas, and A. F. J. Levi, "Adaptive design of nanoscale dielectric structures for photonics," J. Appl. Phys. **94**, 6065–6068 (2003).
10. C. Y. Kao, S. Osher, and E. Yablonovitch, "Maximizing band gaps in two-dimensional photonic crystals by using level set methods," Appl. Phys. B **81**, 235–244 (2005).
11. A. Håkansson, H. T. Miyazaki, and J. Sánchez-Dehesa, "Inverse design for full control of spontaneous emission using light emitting scattering optical elements," Phys. Rev. Lett. **96**, 153902 (2006).
12. L. Shen, Z. Ye, and S. He, "Design of two-dimensional photonic crystals with large absolute band gaps using a genetic algorithm," Phys. Rev. B **68**, 035109 (2003).
13. J. Goh, I. Fushman, D. Englund, and J. Vučković, "Genetic optimization of photonic bandgap structures," Opt. Express **15**, 8218–8230 (2007).
14. A. V. Kildishev, U. K. Chettiar, Z. Liu, V. M. Shalaev, D.-H. Kwon, Z. Bayraktar, and D. H. Werner, "Stochastic optimization of low-loss optical negative-index metamaterial," J. Opt. Soc. Am. B **24**, A34–A39 (2007).
15. P. Y. Chen, C. H. Chen, H. Wang, J. H. Tsai, and W. X. Ni, "Synthesis design of artificial magnetic metamaterials using a genetic algorithm," Opt. Express **16**, 12806–12818 (2008).
16. J. H. Holland, *Adaptation in Natural and Artificial Systems* (MIT Press, 1992).
17. D. E. Goldberg, *Genetic Algorithms in Search, Optimization, and Machine Learning* (Addison-Wesley, 1989).
18. T. Ito and K. Sakoda, "Photonic bands of metallic systems. II. features of surface plasmon polaritons," Phys. Rev. B **64**, 045117 (2001).
19. R. J. Potton, "Reciprocity in optics," Rep. Prog. Phys. **67**, 717–754 (2004).
20. M. Iwanaga, A. S. Vengurlekar, T. Hatano, and T. Ishihara,

"Reciprocal transmittances and reflectances: an elementary proof," Am. J. Phys. **75**, 899–902 (2007).
21. P. B. Johnson and R. W. Christy, "Optical constants of the noble metals," Phys. Rev. B **6**, 4370–4379 (1972).
22. S. G. Tikhodeev, A. L. Yablonskii, E. A. Muljarov, N. A. Gippius, and T. Ishihara, "Quasiguided modes and optical properties of photonic crystal slabs," Phys. Rev. B **66**, 045102 (2002).
23. L. Li, "Use of Fourier series in the analysis of discontinuous periodic structures," J. Opt. Soc. Am. A **13**, 1870–1876 (1996).
24. D. Y. K. Ko and J. C. Inkson, "Matrix method for tunneling in heterostructures: resonant tunneling in multilayer systems," Phys. Rev. B **38**, 9945–9951 (1988).
25. A. Christ, T. Zentgraf, J. Kuhl, S. G. Tikhodeev, N. A. Gippius, and H. Giessen, "Optical properties of planar metallic photonic crystal structures: experiment and theory," Phys. Rev. B **70**, 125113 (2004).
26. M. C. Hutley and D. Maystre, "The total absorption of light by a diffraction grating," Opt. Commun. **19**, 431–436 (1976).
27. T. V. Teperik, F. J. G. de Abajo, A. G. Borisov, M. Abdelsalam, P. N. Bartlett, Y. Sugawara, and J. J. Baumberg, "Omnidirectional absorption in nanostructured metal surfaces," Nat. Photonics **2**, 299–301 (2008).
28. A. Christ, O. J. F. Martin, Y. Ekinci, N. A. Gippius, and S. G. Tikhodeev, "Symmetry breaking in a plasmonic metamaterial at optical wavelength," Nano Lett. **8**, 2171–2175 (2008).
29. S. Collin, F. Pardo, R. Teissier, and J.-L. Pelouard, "Efficient light absorption in metal-semiconductor-metal nanostructures," Appl. Phys. Lett. **85**, 194–196 (2004).